Biophysical Journal
Article

Biophysical Society

Blocking of Single α-Hemolysin Pore by Rhodamine Derivatives

Tatyana I. Rokitskaya,[1,*] Pavel A. Nazarov,[1] Andrey V. Golovin,[2] and Yuri N. Antonenko[1]
[1]Belozersky Institute of Physico-Chemical Biology and [2]Faculty of Bioengineering and Bioinformatics, Lomonosov Moscow State University, Moscow, Russia

ABSTRACT Measurements of ion conductance through α-hemolysin pore in a bilayer lipid membrane revealed blocking of the ion channel by a series of rhodamine 19 and rhodamine B esters. The longest dwell closed time of the blocking was observed with rhodamine 19 butyl ester (C4R1), whereas the octyl ester (C8R1) was of poor effect. Voltage asymmetry in the binding kinetics indicated that rhodamine derivatives bound to the stem part of the aqueous pore lumen. The binding frequency was proportional to a quadratic function of rhodamine concentrations, thereby showing that the dominant binding species were rhodamine dimers. Two levels of the pore conductance and two dwell closed times of the pore were found. The dwell closed times lengthened as the voltage increased, suggesting impermeability of the channel for the ligands. Molecular docking analysis revealed two distinct binding sites within the lumen of the stem of the α-hemolysin pore for the C4R1 dimer, but only one binding site for the C8R1 dimer. The blocking of the α-hemolysin nanopore by rhodamines could be utilized in DNA sequencing as additional optical sensing owing to bright fluorescence of rhodamines if used for DNA labeling.

INTRODUCTION

The *Staphylococcus aureus* α-hemolysin (αHL) channel has been rigorously studied over the last three decades and a lot of functional properties (1,2) and structural details (3) of this protein have been described. Membrane-bound monomers of αHL associate to form heptameric mushroom-shaped transmembrane pores (3,4) comprising a cap, a stem, and seven rim domains. The large dimension (diameter ranges from 14 to 46 Å depending on the transverse position) and stability of the αHL channel encourages the use of this pore in the study of chemical reactions on the level of single molecules (5) and in biotechnology (6–8). The use of a nanopore for sensing at a single molecule level implies that the nanopore should not exhibit gating on its own and that the residence time of the molecule in the pore exceeds the time of its electrodiffusion through the pore. The chemical affinity between αHL channel embedded in planar lipid bilayer membranes and a variety of analytes has permitted the detection and quantification of H^+ and D^+ ions (9,10), small organic molecules (11), divalent cations (12), and poly(ethylene glycol) (13,14).

Currently, two major approaches on the basis of the αHL pore are considered for DNA sequencing. One way involves the use of a modified nanopore with a covalently attached adaptor, which can continuously identify unlabeled nucleoside 5′-monophosphate molecules with high accuracy (15,16). Each base would be registered by a characteristic decrease in pore current amplitude. In this approach, the exonuclease must be in close proximity to the nanopore sensor and must route the released 2′-deoxynucleoside 5′-monophosphate in the nanopore entrance. Another way is to define four different-sized tags that represent the nucleotides during a controlled DNA synthesis by polymerase (17). The tags are released from 5′-phosphate-modified nucleotides and enter a nanopore in release order. This produces a unique ionic current blockage due to the tag's distinct chemical structure.

Although tags based on poly(ethylene glycol)s showed promising results (17), a screening of tags of different structures remained an actual task. Special attention should be paid to fluorescent compounds that can supplement electrophysiological measurements with optical sensing that can be used for verification of the recognition based on electrical traces. One can use, for example, the FRET signal from donor-labeled αHL protein to the tags, with the tags being able to serve as acceptors of the energy and emitting a fluorescent signal. Simultaneous recordings of electrical and optical signals on the single channel level were shown for gramicidin A channel (18–20) and αHL channel (21). Rhodamines exhibiting a high molar extinction coefficient and a high quantum yield of fluorescence are widely used as a fluorescent marker

Submitted February 3, 2017, and accepted for publication April 25, 2017.
*Correspondence: rokitskaya@genebee.msu.ru
Editor: Joseph Mindell.
http://dx.doi.org/10.1016/j.bpj.2017.04.041

and a component of FRET systems (22). The cationic nature of these molecules and their ability to permeate through lipid membranes makes several rhodamine derivatives (e.g., tetramethylrhodamine ethyl ester; TMRE, and others) selective probes for mitochondria because of the inside-negative electrical potential on these intracellular organelles (23). In this work, we showed that esters of different alkyl chain length of rhodamine 19 (Fig. S1 *A*) as well as the esters of rhodamine B (Fig. S1 *B*) can block the αHL channel. The binding of hydrophilic derivatives of the rhodamines to αHL led to two levels of the pore conductances suggesting the presence of two distinct binding sites. The first sublevel, 1C, was ∼25% of the intrinsic pore conductance, whereas the conductance of the second sublevel, 2C, was close to zero, with frequent fluctuations between these two levels. These two types of blocking events varied greatly in the dwell closed times depending on the length of the alkyl chain linked to the rhodamines. Dwell open time of the protein pore was inversely proportional to the quadratic function of rhodamines' concentration. This finding suggested that the binding events were represented by the dimers of the rhodamine derivatives. Rhodamines are known to form dimers even at low concentrations and it was shown that their binding to proteins proceeds in a dimeric form, as in the case of iodoacetamidotetramethylrhodamine and myosin (24). It was shown also in this work that, hydrophobic derivatives of rhodamine 19 carrying long alkyl chain length induced only short blocking events while interacting with αHL. Molecular docking confirmed the ability of C_4R1 and other rhodamine derivatives to bind to the channel lumen and provide mechanistic insights into the channel blocking mechanism. Thus, we uncover a fluorescent blocker of the αHL channel known to be suitable for different nanotechnology applications.

MATERIALS AND METHODS

Chemicals

Rhodamine 19 ethyl ester (C_2R1 or Rhodamine 6G) was purchased from Sigma-Aldrich (St. Louis, MO). Rhodamine 19 derivatives (C_4R1, C_8R1, and C_{12}R1) were synthesized as described in Rokitskaya et al. (25). Ethyl and butyl esters of rhodamine B were prepared by Galina Korshunova and Stepan Denisov (Belozersky Institute, Moscow State University, Russia) as described in Fierz-David and Rufener (26).

All other chemicals were purchased.

Bacterial strains and plasmids

We used *E. coli* strain JM109 (DE3) (Promega, Madison, WI) and pT7 vector (Sigma-Aldrich) carrying 6His-tagged full-length α-Hemolysin from *S. aureus* (pT79/αHL). The vector pT7 containing α-Hemolysin was a generous gift of Dr. H. Bayley, University of Oxford, Oxford, UK.

Expression of α-hemolysin proteins

Competent bacteria were transformed with the recombinant plasmids by standard procedures. A colony was transferred from a petri dish into 5 mL of LB liquid medium containing ampicillin (100 mg/mL), and cultivated overnight at 37°C. The culture was diluted 1:100 with fresh LB medium (500 mL, ampicillin 100 mg/mL). Gene expression was induced by adding IPTG (0.5 mM) into the growth medium. The culture was then incubated for 6 h at 28°C with shaking at 140 rpm.

Protein purification

Bacteria were harvested by centrifugation (7500 × *g*, 10 min), and washed with PBS pH 7.4 and centrifuged for 15 min at 3500 × *g*. The sediment was suspended in 12 mL of cooled lysis buffer with 0.5 mM PMSF (50 mM sodium phosphate, 0.5 M NaCl, pH 8.0). The bacteria were disrupted using a French press (maximum pressure of 8 t per cm^2) and debris was removed by centrifugation for 15 min at 15,000 × *g*. To sediment inclusion bodies, the supernatant was centrifuged for 15 min at 39,000 × *g*. The resulting supernatant was loaded to column with Profinity IMAC Ni-charged resin (Bio-Rad, Hercules, CA) and αHL protein was purified under nondenaturation conditions by gravity flow protocol. For quality control of purification, sodium dodecyl sulfate-polyacrylamide gel electrophoresis analysis of a representative 6His-tagged αHL was conducted as described in Laemmli (27) (data not shown).

Lipid bilayer technique

Planar bilayer lipid membranes (BLM) were formed from a 2% solution of diphytanoylphosphatidylcholine (Avanti Polar Lipids, Alabaster, AL) in *n*-decane on a hole in a Teflon partition (0.25-mm diameter) separating two compartments of a cell containing aqueous buffer solutions (28). 1 M KCl, 10 mM Tris, 10 mM MES, pH = 7.5 was used as the electrolyte. The experiments were carried out at room temperature (23–25°C). Small amounts of αHL were added from the *cis*-side of the cell (side connected to ground electrode). Spontaneous channel insertion was obtained while stirring under applied voltage. Voltage was applied to BLMs with Ag-AgCl electrodes placed into the solutions on the two sides of the BLM via agar bridges. The electric current was recorded under voltage-clamp conditions by means of a patch-clamp amplifier (model No. BC-525C; Warner Instruments, Hamden, CT). Signals were filtered by a low-pass Bessel filter at 500 Hz and digitized using an NI-DAQmx (National Instruments, Austin, TX) with a sampling frequency of 10 kHz. Single channel analysis was performed using WinEDR Strathclyde Electrophysiology Software designed by J. Dempster (University of Strathclyde, Glasgow, UK). Blockage times were calculated by fitting logarithmic double exponentials to logarithmically binned histograms (29).

Docking simulation and analysis

Based on the known property of rhodamine to form dimers even at low concentrations (24), we designed the geometry of the dimer using the method of DFTB3 (30) with dispersion D3 (31) and parameters 3OB (32). The resulting geometry was used to construct the ligand topology for use in AutoDock Vina (33). Description of the protein was prepared using OpenBabel (34). Docking of rhodamines was carried out in cells of 30, 30, and 70 Å each with the center at 0.3, −2.7, and 10.3 of the initial protein coordinates (PDB:7AHL). To reach the optimal scanning of the cell space, we used an exhaustiveness of 64 and the program was run 200 times. The analysis of the results was performed with the help of PYTHON modules (https://www.python.org/). Images were prepared with the software PyMOL (PyMOL Molecular Graphics System, Version 1.8; https://www.pymol.org).

RESULTS

Purified αHL was added to a final concentration of 10−50 ng/mL. The stirring of the membrane bathing

solution was prolonged until a single channel inserted into the membrane. According to Song et al. (3), the protein incorporation proceeded in a way that the channel stem faced the *trans* side whereas the channel vestibule faced the *cis* side. The channel conductance under our experimental conditions was 1.01 ± 0.05 nS and 0.84 ± 0.03 nS (n = 9) for voltages +50 mV and −50 mV, respectively (1 M KCl, 10 mM MES, and 10 mM Tris pH = 7.5). These values were in good agreement with that of others (5,35). Rhodamine 6G (C_2R1) and other compounds was added at two sides of the membrane; however, its initial symmetrical distribution should be distorted after the application of transmembrane voltage because of the permeability of these cationic compounds through the membrane (36). The addition of C_2R1 or C_4R1 to the membrane reconstituted with single αHL pore led to well-defined blocking events with characteristic duration in the range of tens of milliseconds (Fig. 1, *B* and *C*), whereas no blocking was observed without rhodamines at +50 mV (Fig. 1 *A*). It should be stressed that it was important to perform thorough and prolonged stirring of the solution after the addition of rhodamines to obtain reproducible results because of limited aqueous solubility of some derivatives. In contrast to C_2R1 or C_4R1 (Fig. 1 *C*), the effects of C_8R1 (Fig. 1 *D*) and $C_{12}R1$ (Fig. 1 *E*) were much less pronounced, resulting in a brief flickering of the current. The inset to Fig. 1 *B* shows that in case of C_2R1, there were

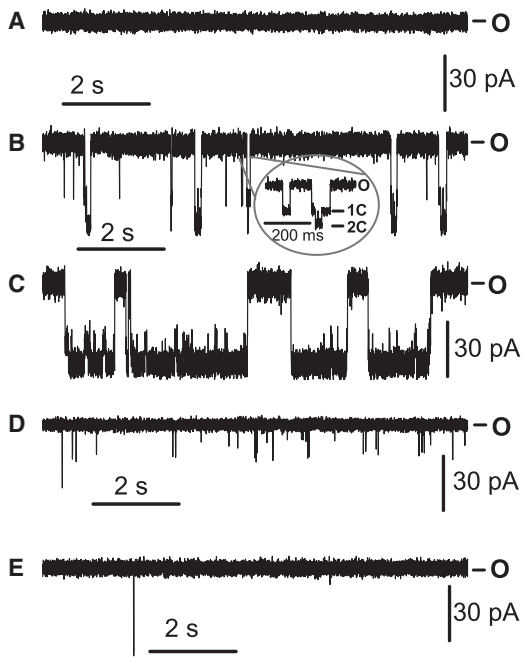

FIGURE 1 Shown here are the traces of current through the single αHL channel without rhodamines (*A*) or in the presence of 20 μM C_2R1 (*B*), 20 μM C_4R1 (*C*), 15 μM C_8R1 (*D*), or 20 μM $C_{12}R1$ (*E*). The inset to (*B*) demonstrates in more detail two blocking states of the channel (1C and 2C). The applied potential was +50 mV.

two blocking states of the channel with frequent transitions to deeper blocking state 2C through intermediate blocking state 1C. Among the rhodamine 19 derivatives studied, the most pronounced effect was in case of C_4R1, where the channel dwelled more time in the closed states at 20 μM of the compound (Fig. 1 *C*). Thus, the blocking of the αHL channel exhibited clear nonmonotonic dependence on the alkyl chain length of the rhodamine esters.

Interestingly, the α-Hemolysin channel was not blocked by several other fluorescent compounds such as fluorescein or carboxyfluorescein. For example, even 60 μM of fluorescein produced only rare short blocking events of <1 ms duration (data not shown). Apparently these dyes do not bind to the pore wall, which is a mandatory requirement for the sensing in this system (37).

C_2R1 and other rhodamine derivatives can induce electrical current through lipid membranes owing to their membrane permeability (36). This phenomenon was thoroughly studied in our laboratory for the case of $C_{12}R1$ (38). To determine the completeness of the blocking of the 2C state, the experiments were carried out with low concentrations of C_4R1 (5 μM) (Fig. 2 *A*) that did not induce the BLM current by itself while blocking the channel quite frequently to 1C and 2C states (*inset* to Fig. 2 *A*). The current histogram shows that the 2C state of the αHL pore was close to zero conductance. The blockage current histogram was analyzed as three Gaussian distributions (Fig. 2 *B*, *gray curve*) with positions of the peaks and width of distributions—0 ± 3.4 pA, 11.8 ± 3.3 pA, and 47.9 ± 3.3 pA. The conductance of 1C comprised 24.5% of the full αHL conductance. Despite symmetrical addition of C_4R1, the blocking was highly asymmetrical with respect to the applied voltage and was almost absent at −50 mV (Fig. 2 *C*), where only rare brief flickering events were observed.

A binding kinetics of the ligands can be quantified by two characteristics: τ_{on} (open time) and τ_{off} (blockage time). Histograms displaying the dwell open time of αHL depended considerably on the concentration of C_2R1 and could be fitted well by single-exponential (Fig. 3 *A*) curves with characteristic time τ_{on} decreasing with the increase in the concentration of C_2R1. Fig. 3 *B* presents the dependence of the inverse mean dwell open time τ_{on} on C_2R1 concentration in logarithmic coordinates. We found that the reciprocal of τ_{on} was an almost quadratic function of the ligand concentration. These results were approximated by a power function, $[C_2R1]^n$, with $n = 2.2$ suggesting involvement of C_2R1 dimers in the blocking events.

It can be seen from the current traces in Fig. 4 *B* that the dwell time of C_4R1 blocking was different for 1C and 2C states. Log-binned dwell time histograms (29) for C_2R1 and C_4R1 binding in the lumen of the pore (τ_{off}) at logarithmic scale are presented in Fig. 4 *A* for the data obtained at +50 mV. The histograms are well represented by the sum of two exponentials with substantially different characteristic times ($\tau_{off}1$ and $\tau_{off}2$, Fig. 4 *B*). The following values

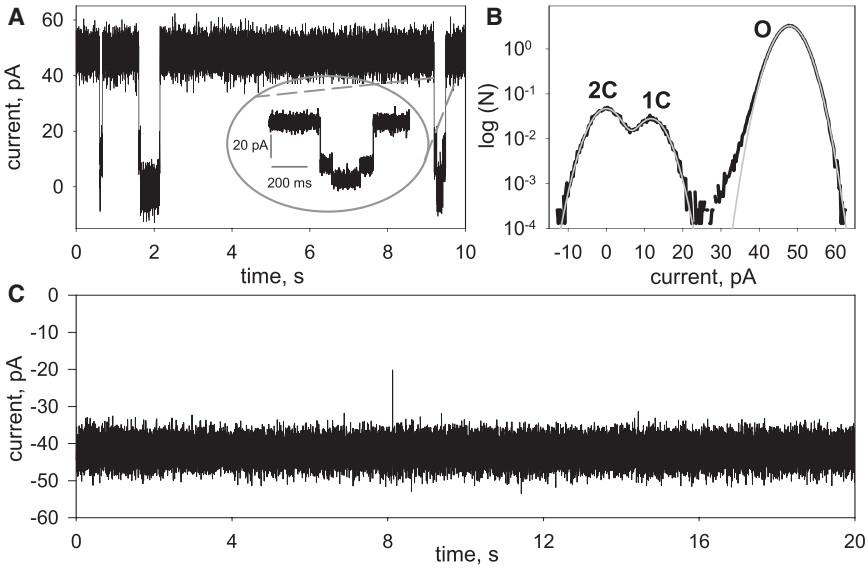

FIGURE 2 (*A*) Shown here are the traces of the current through the single αHL channel in the presence of 5 μM C_4R1 at the applied potential +50 mV (*A*) or −50 mV (*C*). (*B*) Representative current amplitude histogram of the recording at +50 mV was fitted by a sum of three Gaussians (*gray curves*). Positions of the peaks and widths of distributions are 0 ± 3.4 pA (marked *2C*), 11.8 ± 3.3 pA (marked *1C*) and 47.9 ± 3.3 pA (marked *O*).

of $\tau_{off}1$ and $\tau_{off}2$ were determined: 12 ms and 180 ms in case of C_2R1; 18 ms and 880 ms in case of C_4R1, respectively. Thus, the C_4R1 times were substantially longer than those of C_2R1. $\tau_{off}1$ and $\tau_{off}2$ depended poorly on the concentration of the ligands (data not shown). The above described quantitative analysis of the blocking events could hardly be applied to the case of fast blocking events induced by C_8R1 and C_{12}R1. However, the estimated average blocking time was 1.7 and 1.3 ms for C_8R1 and C_{12}R1, respectively (+50 mV, data not shown). The estimated average blocking times of the interaction of the rhodamines with αHL ($\tau_{off}1$ and $\tau_{off}2$) are summarized in Table 1.

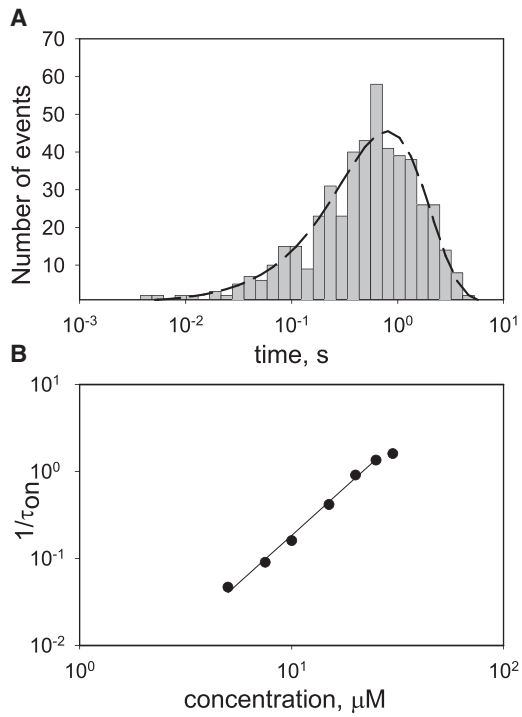

FIGURE 3 (*A*) Shown here is the log-binned dwell open time histogram of the single αHL pore with approximation by a single exponent in the presence of 25 μM C_2R1 (τ_{on} = 0.77 s). The applied potential was +50 mV. (*B*). Shown here is the inverse mean dwell open time ($1/\tau_{on}$) of the αHL channel as a function of C_2R1 concentration. The line represents approximation of the data by the power function $[C_2R1]^n$ with n = 2.2.

Fig. 4 *C* shows the plot of the probability of being unblocked versus voltage in the presence of 10 μM C_4R1. This parameter was estimated from the areas under the current histograms at different voltages. The dependences of open dwell time (τ_{on}, *solid circles*), $\tau_{off}1$ (*dotted circles*), and $\tau_{off}2$ (*open circles*) on the voltage are shown in Fig. 4 *D*. It can be concluded that the blocking occurred upon the cationic rhodamine entering from the *trans* side of the membrane (opposite to the side of addition). The observed increase in the time of the ligand binding to the channel ($\tau_{off}1$ and $\tau_{off}2$) upon the increase in the voltage favors intercalation rather than translocation of ligand through the channel. As it has been shown previously, translocation and intercalation events are expected to have similar blockage currents but the effect of voltage should be opposite (39,40). In fact, the duration of electrophoretically driven binding events for a translocation process is expected to decrease as the voltage increases. It is interesting that open dwell time τ_{on} poorly depended on the applied voltage (*solid circles* in Fig. 4 *D*), suggesting that this process depended on the extrachannel concentration of the ligand. It was shown early for the NfpA/NfpB channel from *Nocardia farcinica* that its blockage time by hepta- and penta-arginine increased with increasing voltage, which indicated that polyarginines just bind to the channel without effective translocation (41). The increase of voltage above some

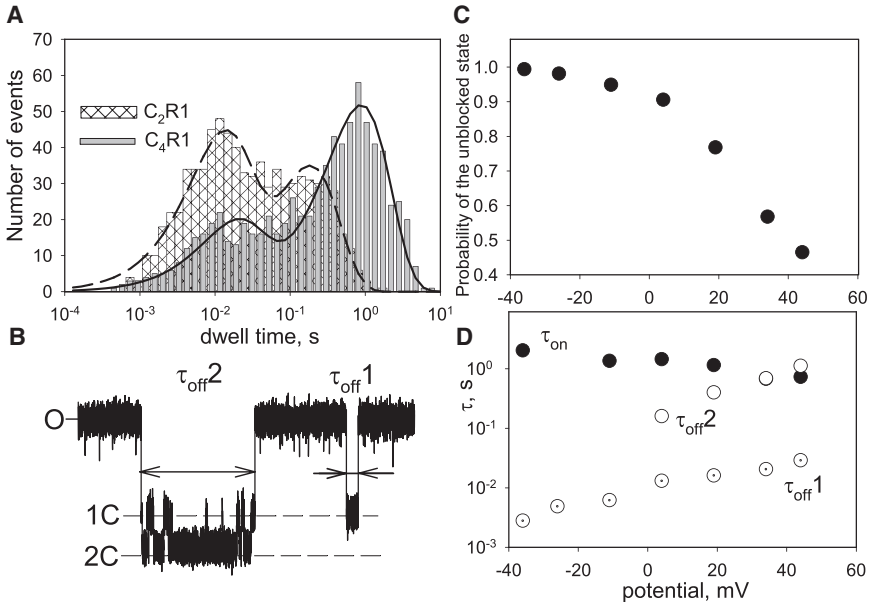

FIGURE 4 (*A*) Shown here are the log-binned dwell blockage time histograms for C_2R1 and C_4R1 binding with the single αHL channel. Distributions of blockage times were analyzed by logarithmic double exponential fitting ($\tau_{off}1 = 12$ ms and $\tau_{off}2 = 0.18$ s for C_2R1, *medium dashed line*; $\tau_{off}1 = 18$ ms and $\tau_{off}2 = 0.88$ s for C_4R1, *solid line*). (*B*) Shown here is a trace of the current through the single αHL pore in the presence of 10 μM C_4R1, demonstrating, in detail, two blocked states of the pore designating two types of events corresponding to $\tau_{off}1$ and $\tau_{off}2$. (*C*) Shown here is the probability of the single αHL channel being in unblocked state versus applied potential in the presence of 10 μM C_4R1. (*D*) Shown here is the dependence of τ_{on} (*solid circles*), $\tau_{off}1$ (*dotted circles*), and $\tau_{off}2$ (*open circles*) on BLM voltage in the presence of 10 μM C_4R1.

threshold level was shown to decrease the average residence time, suggesting translocation of the peptide through the NfpA/NfpB channel. Unfortunately, we could not check the effect of large voltages in our experiments. Voltage exceeding 50 mV in the presence of rhodamine derivatives often triggered a channel into a low-conductance state. The ability of the αHL pore to fluctuate between high- and low-conductance states was shown previously for high transmembrane potentials ($V \geq \pm$ 100 mV) (42).

As shown in Fig. S1, the structure of rhodamine B is close to rhodamine 19 but it lacks the ability to lose a proton at alkaline pH (43) and the molecule possesses permanent positive charge. Fig. 5 *A* shows a current trace through a single αHL channel in the presence of 15 μM C_2RB at +50 mV. The blocking by C_2RB was similar to that of C_2R1 exhibiting two levels C1 and C2 (*inset* to Fig. 5 *A*). At negative potentials, the blocking by C_2RB was substantially less pronounced (Fig. 5 *C*). The C1 and C2 blocking times $\tau_{off}1$ and $\tau_{off}2$ were smaller compared to that of rhodamine 6G (6 and 24 ms, respectively, as determined from the log-binned dwell time histogram). In the case of C_4RB, the $\tau_{off}1$ and $\tau_{off}2$ were 15 and 72 ms, correspondingly (Fig. 5 *B*). The blocking by C_2RB (Fig. 5 *A*) as well as by C_4RB (data not shown) can be characterized by the presence of small amplitude flickering (<20% of the channel conductance) with times <1 ms. These events were absent at negative voltages (Fig. 5 *C*). It can be proposed that these fast blocking events corresponded to the interaction of the C_2RB and C_4RB with the outside of the pore and diffusion away the pore, i.e., to bumping events (39). Based on the voltage dependence of the small amplitude blocking events, they should be a result of the interaction of the ligands with the stem-base part of the pore, most probably with a ring of acidic residues formed by D128 (3).

TABLE 1 The Times of Rhodamines and their Derivative Binding Events Measured with the Single α-Hemolysin Channel at +50 mV

Compound	$\tau_{off}1$, ms	$\tau_{off}2$, ms
C_2R1	12 ± 2	180 ± 30
C_4R1	20 ± 5	800 ± 150
C_8R1	1.7 ± 0.3	—
$C_{12}R1$	1.3 ± 0.3	—
C_2RB	5 ± 1.2	20 ± 4
C_4RB	16 ± 3	57 ± 15

Mean ± SD for three experiments for each compound.

DISCUSSION

It has been shown in this work that fluorescent cations based on rhodamine 19 and rhodamine B blocked the αHL channel at concentrations lower or comparable to other known ligands (organic molecules (11), polypeptides (44,45), crown ether (46), nonionic polymers (47), or flavonoids (35)). The blocking by the rhodamines led to two substates 1C and 2C (Figs. 1 *B*, 2 *A*, and 5 *A*) with transitions between them. The conductance of 1C comprised 24.5% of the fully open state whereas the conductance of 2C was close to zero. The inverse mean dwell open time presented a quadratic dependence on concentration of the ligands ($n = 2.2$ for C_2R1 Fig. 3 *B*; $n = 1.9$ for C_4R1 (data not shown) and $n = 1.9$ for C_2RB (data not shown), suggesting the binding of two molecules with the pore. It has been shown previously that rhodamines are able to form dimers in aqueous solutions (48,49), and a likely conformation of the rhodamine

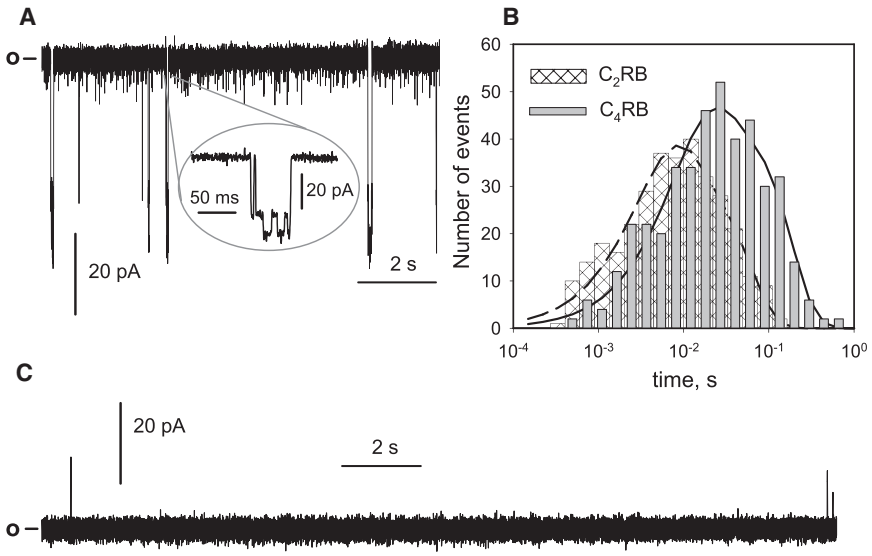

FIGURE 5 Shown here are the traces of the current through the single αHL channel in the presence of 15 μM C_2RB at applied potential +50 mV (*A*) or −50 mV (*C*). The inset to (*A*) demonstrates in more detail the blocking states of the channel. (*B*) Shown here are the log-binned dwell blockage time histograms for C_2RB and C_4RB binding with the single αHL channel. Distributions of blockage times were analyzed by logarithmic double exponential fitting ($\tau_{off}1 = 6$ ms and $\tau_{off}2 = 24$ s for C_2RB, *medium dashed line*; $\tau_{off}1 = 15$ ms and $\tau_{off}2 = 72$ ms for C_4RB, *solid line*).

B and rhodamine 6G homodimers was proposed on the basis of two-dimensional proton-proton nuclear Overhauser enhancement spectroscopy (50). It can be assumed, therefore, that the blocking of the αHL channel by rhodamines occurred by their dimers.

We conducted a computer simulation of the process of blocking of the αHL pore by rhodamines using the method of molecular docking and found that the dimeric forms of C_2R1, C_4R1, and C_8R1 were able to bind to the stem part of the pore. Fig. 6 shows side views (*top*) and views from below (*bottom*) for the results of the simulation for the positions of C_2R1, C_4R1, and C_8R1 in the pore. Fig. 6 *B* shows clearly that the dimers did not fill the lumen completely, and even in the case of bulky C_8R1 nearly half of the pore remained open. Docking of monomers did not provide any specific binding sites (data not shown).

We estimated the probability of finding dimers of rhodamine molecules in certain sites of the channel by exploiting wide sampling in simulations. Fig. 7 *A* shows the results as maps of atom density, for bridging oxygen atoms in the rhodamines under study. Blue and yellow colors mean higher and lower probability, respectively. A probability-distance histogram of the dimers with respect to the center of the membrane is shown in Fig. 7 *B*. The histogram highlights the possibility of the binding of all three dimers at the pore entrance, from 7 to 11 Å

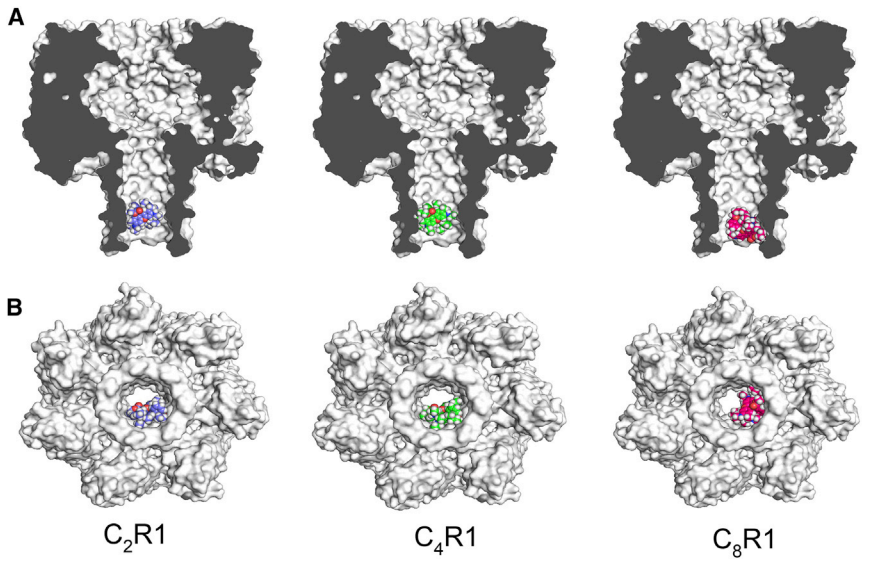

FIGURE 6 Shown here are the locations of rhodamine derivative binding sites in the αHL pore down the membrane center (*A*, *side view*; *B*, *bottom view*). The dimer of the rhodamine derivatives is marked in blue for C_2R1, green for C_4R1, and red for C_8R1. To see this figure in color, go online.

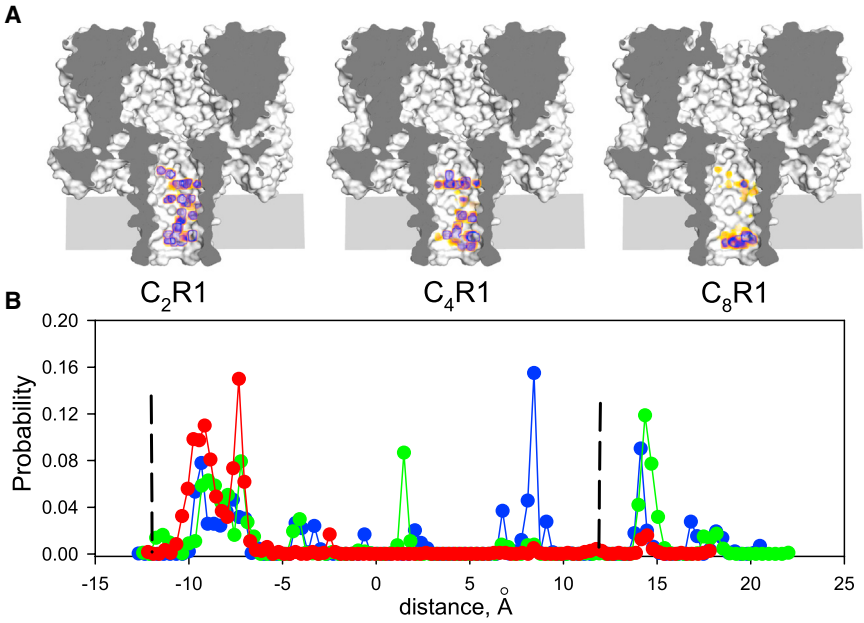

FIGURE 7 (*A*) Shown here is the density of location of the bridging oxygen atoms of the rhodamines dimer in the αHL pore. Blue and yellow colors mean higher and lower probability, respectively. (*B*) Shown here are the histograms of the distribution of the docking occurrence in the αHL pore on the distance from the membrane center. The borders of the lipid bilayer are marked by black dashed lines. The dimer of the rhodamine derivatives is marked in blue for C_2R1, green for C_4R1, and red for C_8R1. To see this figure in color, go online

down the membrane center (amino acids D127 and G133, Fig. 7 *B*). Besides, whereas C_2R1 and C_4R1 had additional binding sites (they had a common binding site at the distance of 15 Å above the center of the membrane near amino acids T117 and G119), the C_8R1 analog did not have binding sites near the central constriction of the channel lumen (Fig. 7 *B*).

Our in silico experiments provided a rationale for the C1 blocking state of the αHL channel pointing to the rhodamine binding to the pore, down the membrane center, as a probable mechanism for the C1 substate. However, the simulations failed to explain the full closure of the channel in the 2C substate. It can hardly be assumed that the additional binding sites near the central constriction of the lumen can be related to the 2C state because the molecular volumes of the dimers of C_2R1 and C_4R1 are too small to fill the whole αHL pore even at this narrow site (Fig. S2). To shed light on the mechanism of the C2 substate, one can consider recent works of molecular dynamics simulation of the αHL pore with a modified pore interior leading to impeding of the flow of water molecules or ions through the pore due to dewetting of the pore interior (51,52). The modification included the introduction of leucine amino acids and narrowing the open pore minimum diameter to 9 Å. According to our docking analysis, the width of the channel lumen was ∼10 Å upon C_2R1 binding in the central constriction of the lumen (Fig. S2). The process of dewetting under these conditions could be promoted by hydrophobic properties of the rhodamine molecule having an octanol-water partition coefficient (*Log*P) of 2.37 (53). The increase in the duration of the C2 substate ($\tau_{off}2$) for C_4R1 compared to C_2R1 (Table 1) can be related to the differences in their sizes or/and hydrophobicities. It can be noted that short additional blockades of the $(M113N)_7$-α-HL pore during the interaction with βCD were observed earlier (54), and that this process was more pronounced at high temperatures (55).

The binding of the second rhodamine dimer in the αHL pore as a mechanism of the 2C substate actually contradicted frequently observed transitions from the O to 2C states without an intermediate 1C substate. For example, these transitions are seen in Fig. 1, *B* and *C*. It is interesting also to analyze the concentration dependence of the 1C–2C transitions for C_4R1 because the events of the binding of the second dimer should lead to the steep concentration dependence of their occurrence. Experiments showed that at 5 μM C_4R1, the duration of 1C was $\tau_{1C} = 42.5 \pm 7$ ms, whereas $\tau_{2C} = 150 \pm 29$ ms. The increase in the concentration of C_4R1 up to 20 μM led to $\tau_{1C} = 23.5 \pm 3$ ms and $\tau_{2C} = 160 \pm 23$ ms (examples of these events are presented in Fig. S3). Therefore, the increase in the C_4R1 concentration by fourfold (and dimers by 16-fold as $[dimerC_4R1] \sim [C_4R1]^2$) led to the increase in the 1C–2C transitions by less than twofold. This poor concentration dependence also argued against the hypothesis of the simultaneous binding of two dimers to the channel.

As far as the process of rhodamine dimerization was rigorously studied, we applied a known dimerization equilibrium constant for R6G (C_2R1) (48,49,56) for evaluation of the rate constant of association of the R6G dimer with the αHL pore. For this purpose, a mean value for K_d (∼4000 M^{-1}) in aqueous solution was chosen (56) that was close to the value in 1 M KCl (49). The rate constant of association k_{on} can be

derived from the slopes of plots of $1/\tau_{open}$ versus [dimerC_2R1], where [dimerC_2R1] is the dimer concentration in aqueous solution and [dimerC_2R1] = K_d*[C_2R1]^2. The value of k_{on} was 5.4 × 10^5 $M^{-1}s^{-1}$ and close to the rate constant of βCD interaction with the αHL pore (57).

CONCLUSIONS

In this work we showed that the dimers of alkylated Rhodamine 19 and rhodamine B can block the single αHL channel and the blockage time differed for the types of rhodamines and the length of the alkyl chain. More hydrophilic derivatives of the rhodamines caused closure of the αHL pore more efficiently, and the blocking displayed two conductance states: one was approximately one-quarter of the initial conductance, and the second was close to zero. Histograms of dwell blocking time demonstrated two different durations of blocking, obviously revealing various blocking processes. The most prolonged time was observed in the presence of C_4R1 (~1 s). Hydrophobic derivatives (C_8R1 and C_{12}R1) produced just brief closure (characteristic times were approximately a millisecond). It is interesting to mention in this connection that the interaction of C_4R1 with the carrier protein of the inner mitochondrial membrane leading to mitochondrial uncoupling was also considerably stronger than that of C_8R1 and C_{12}R1 (58). The asymmetry in the voltage dependence of the blocking times revealed that rhodamine derivatives can enter and block the channel from its stem part but cannot translocate through the pore. Docking of the rhodamine dimers indicated differences in specific binding sites for C_nR1, depending on the hydrophobicity of rhodamine derivatives. By comparing the electrophysiological data and the simulations, we concluded that the occupied state of the pore, in the presence of hydrophilic derivatives with prolonged fluctuation between two levels of conductivities, corresponded to single binding of the rhodamine dimers near the central constriction of the pore. Fluctuations could be related to the rotation of the ligand in the binding site or dewetting mechanism in the narrow lumen of the binding site. In the latter case, the closed state of the pore is not occluded, but is sufficiently hydrophobic and narrow to energetically exclude water molecules and ions from the pore, as it was proposed in Beckstein and Sansom (59). The results shown here should be helpful in designing inhibitors of toxins and protein channels that frequently play a key role in the impact of pathogenic bacteria on mammalian cells as found previously for cyclodextrin derivatives and αHL (60,61).

SUPPORTING MATERIAL

Three figures are available at http://www.biophysj.org/biophysj/supplemental/S0006-3495(17)30457-5.

AUTHOR CONTRIBUTIONS

Y.N.A. initiated research. P.A.N. performed the protein expression and purification. T.I.R. and Y.N.A. designed experiments. T.I.R. and A.V.G. performed research and analyzed the data. T.I.R. and Y.N.A. wrote the article.

ACKNOWLEDGMENTS

The authors thank Dr. Galina Korshunova and Stepan Denisov for preparation of rhodamine derivatives and Dr. Elena Kotova for valuable comments.

This work was partially supported by the Russian Foundation for Basic Research grant No. 15-04-01688 (electrophysiological studies), the Russian Science Foundation grant No. 16-14-10025 (design of rhodamine derivatives), and the Russian Science Foundation grant No. 14-50-00029 (docking analysis).

REFERENCES

1. Menestrina, G. 1986. Ionic channels formed by *Staphylococcus aureus* α-toxin: voltage-dependent inhibition by divalent and trivalent cations. *J. Membr. Biol.* 90:177–190.
2. Krasilnikov, O. V., and R. Z. Sabirov. 1989. Ion transport through channels formed in lipid bilayers by *Staphylococcus aureus* α-toxin. *Gen. Physiol. Biophys.* 8:213–222.
3. Song, L., M. R. Hobaugh, …, J. E. Gouaux. 1996. Structure of staphylococcal α-hemolysin, a heptameric transmembrane pore. *Science.* 274:1859–1866.
4. Gouaux, J. E., O. Braha, …, H. Bayley. 1994. Subunit stoichiometry of staphylococcal α-hemolysin in crystals and on membranes: a heptameric transmembrane pore. *Proc. Natl. Acad. Sci. USA.* 91:12828–12831.
5. Bayley, H., and P. S. Cremer. 2001. Stochastic sensors inspired by biology. *Nature.* 413:226–230.
6. Kasianowicz, J. J., E. Brandin, …, D. W. Deamer. 1996. Characterization of individual polynucleotide molecules using a membrane channel. *Proc. Natl. Acad. Sci. USA.* 93:13770–13773.
7. Kasianowicz, J. J., A. K. Balijepalli, …, J. W. Robertson. 2016. Analytical applications for pore-forming proteins. *Biochim. Biophys. Acta.* 1858:593–606.
8. Kasianowicz, J. J., and S. M. Bezrukov. 2016. On 'three decades of nanopore sequencing'. *Nat. Biotechnol.* 34:481–482.
9. Bezrukov, S. M., and J. J. Kasianowicz. 1993. Current noise reveals protonation kinetics and number of ionizable sites in an open protein ion channel. *Phys. Rev. Lett.* 70:2352–2355.
10. Kasianowicz, J. J., and S. M. Bezrukov. 1995. Protonation dynamics of the α-toxin ion channel from spectral analysis of pH-dependent current fluctuations. *Biophys. J.* 69:94–105.
11. Gu, L. Q., O. Braha, …, H. Bayley. 1999. Stochastic sensing of organic analytes by a pore-forming protein containing a molecular adapter. *Nature.* 398:686–690.
12. Kasianowicz, J. J., D. L. Burden, …, H. Bayley. 1999. Genetically engineered metal ion binding sites on the outside of a channel's transmembrane β-barrel. *Biophys. J.* 76:837–845.
13. Robertson, J. W., C. G. Rodrigues, …, J. J. Kasianowicz. 2007. Single-molecule mass spectrometry in solution using a solitary nanopore. *Proc. Natl. Acad. Sci. USA.* 104:8207–8211.
14. Reiner, J. E., J. J. Kasianowicz, …, J. W. Robertson. 2010. Theory for polymer analysis using nanopore-based single-molecule mass spectrometry. *Proc. Natl. Acad. Sci. USA.* 107:12080–12085.
15. Clarke, J., H. C. Wu, …, H. Bayley. 2009. Continuous base identification for single-molecule nanopore DNA sequencing. *Nat. Nanotechnol.* 4:265–270.
16. Ayub, M., D. Stoddart, and H. Bayley. 2015. Nucleobase recognition by truncated α-hemolysin pores. *ACS Nano.* 9:7895–7903.

17. Kumar, S., C. Tao, …, J. Ju. 2012. PEG-labeled nucleotides and nanopore detection for single molecule DNA sequencing by synthesis. *Sci. Rep.* 2:684.
18. Borisenko, V., T. Lougheed, …, G. J. Schütz. 2003. Simultaneous optical and electrical recording of single gramicidin channels. *Biophys. J.* 84:612–622.
19. Harms, G. S., G. Orr, …, H. P. Lu. 2003. Probing conformational changes of gramicidin ion channels by single-molecule patch-clamp fluorescence microscopy. *Biophys. J.* 85:1826–1838.
20. Lu, H. P. 2008. Combined single-molecule electrical recording and single-molecule spectroscopy studies of ion channel conformational dynamics. *Methods Cell Biol.* 90:435–451.
21. Heron, A. J., J. R. Thompson, …, M. I. Wallace. 2009. Simultaneous measurement of ionic current and fluorescence from single protein pores. *J. Am. Chem. Soc.* 131:1652–1653.
22. Dempski, R. E., K. Hartung, …, E. Bamberg. 2006. Fluorometric measurements of intermolecular distances between the α- and β-subunits of the Na^+/K^+-ATPase. *J. Biol. Chem.* 281:36338–36346.
23. Johnson, L. V., M. L. Walsh, and L. B. Chen. 1980. Localization of mitochondria in living cells with rhodamine 123. *Proc. Natl. Acad. Sci. USA.* 77:990–994.
24. Ajtai, K., P. J. Ilich, …, T. P. Burghardt. 1992. Stereospecific reaction of muscle fiber proteins with the 5′ or 6′ isomer of (iodoacetamido)tetramethylrhodamine. *Biochemistry.* 31:12431–12440.
25. Rokitskaya, T. I., N. V. Sumbatyan, …, V. P. Skulachev. 2010. Mitochondria-targeted penetrating cations as carriers of hydrophobic anions through lipid membranes. *Biochim. Biophys. Acta.* 1798:1698–1706.
26. Fierz-David, H. E., and J. P. Rufener. 1934. Zur Kenntnis des Monoathyl-o-toluidins und einiger daraus erhaltlicher Rhodamine. *Helv. Chim. Acta.* 17:1452–1459.
27. Laemmli, U. K. 1970. Cleavage of structural proteins during the assembly of the head of bacteriophage T4. *Nature.* 227:680–685.
28. Mueller, P., D. O. Rudin, …, W. C. Wescott. 1963. Methods for the formation of single bimolecular lipid membranes in aqueous solution. *J. Phys. Chem.* 67:534–535.
29. Sigworth, F. J., and S. M. Sine. 1987. Data transformations for improved display and fitting of single-channel dwell time histograms. *Biophys. J.* 52:1047–1054.
30. Gaus, M., Q. Cui, and M. Elstner. 2012. DFTB3: extension of the self-consistent-charge density-functional tight-binding method (SCC-DFTB). *J. Chem. Theory Comput.* 7:931–948.
31. Kubillus, M., T. Kubař, …, M. Elstner. 2015. Parameterization of the DFTB3 method for Br, Ca, Cl, F, I, K, and Na in organic and biological systems. *J. Chem. Theory Comput.* 11:332–342.
32. Gaus, M., A. Goez, and M. Elstner. 2013. Parametrization and benchmark of DFTB3 for organic molecules. *J. Chem. Theory Comput.* 9:338–354.
33. Trott, O., and A. J. Olson. 2010. AutoDock Vina: improving the speed and accuracy of docking with a new scoring function, efficient optimization, and multithreading. *J. Comput. Chem.* 31:455–461.
34. O'Boyle, N. M., M. Banck, …, G. R. Hutchison. 2011. Open Babel: an open chemical toolbox. *J. Cheminform.* 3:33.
35. Ostroumova, O. S., S. S. Efimova, and L. V. Schagina. 2011. 5- and 4′-Hydroxylated flavonoids affect voltage gating of single α-hemolysin pore. *Biochim. Biophys. Acta.* 1808:2051–2058.
36. Melikyan, G. B., B. N. Deriy, …, F. S. Cohen. 1996. Voltage-dependent translocation of R18 and DiI across lipid bilayers leads to fluorescence changes. *Biophys. J.* 71:2680–2691.
37. Kasianowicz, J. J., J. W. Robertson, …, V. M. Stanford. 2008. Nanoscopic porous sensors. *Annu. Rev. Anal. Chem. (Palo Alto, Calif.).* 1:737–766.
38. Rokitskaya, T. I., T. M. Ilyasova, …, V. P. Skulachev. 2013. Electrogenic proton transport across lipid bilayer membranes mediated by cationic derivatives of rhodamine 19: comparison with anionic protonophores. *Eur. Biophys. J.* 42:477–485.
39. Meng, H., D. Detillieux, …, J. S. Lee. 2010. Nanopore analysis of tethered peptides. *J. Pept. Sci.* 16:701–708.
40. Christensen, C., C. Baran, …, J. S. Lee. 2011. Effect of charge, topology and orientation of the electric field on the interaction of peptides with the α-hemolysin pore. *J. Pept. Sci.* 17:726–734.
41. Singh, P. R., I. Bárcena-Uribarri, …, K. R. Mahendran. 2012. Pulling peptides across nanochannels: resolving peptide binding and translocation through the hetero-oligomeric channel from *Nocardia farcinica*. *ACS Nano.* 6:10699–10707.
42. Korchev, Y. E., C. L. Bashford, …, C. A. Pasternak. 1995. Low conductance states of a single ion channel are not 'closed'. *J. Membr. Biol.* 147:233–239.
43. Antonenko, Y. N., A. V. Avetisyan, …, V. P. Skulachev. 2011. Derivatives of rhodamine 19 as mild mitochondria-targeted cationic uncouplers. *J. Biol. Chem.* 286:17831–17840.
44. Movileanu, L., J. P. Schmittschmitt, …, H. Bayley. 2005. Interactions of peptides with a protein pore. *Biophys. J.* 89:1030–1045.
45. Wolfe, A. J., M. M. Mohammad, …, L. Movileanu. 2007. Catalyzing the translocation of polypeptides through attractive interactions. *J. Am. Chem. Soc.* 129:14034–14041.
46. Bezrukov, S. M., O. V. Krasilnikov, …, C. G. Rodrigues. 2004. Field-dependent effect of crown ether (18-crown-6) on ionic conductance of α-hemolysin channels. *Biophys. J.* 87:3162–3171.
47. Rodrigues, C. G., D. C. Machado, …, O. V. Krasilnikov. 2008. Mechanism of KCl enhancement in detection of nonionic polymers by nanopore sensors. *Biophys. J.* 95:5186–5192.
48. Selwyn, J. E., and J. I. Steinfeld. 1972. Aggregation of equilibria of xanthene dyes. *J. Phys. Chem.* 76:762–774.
49. Ghasemi, J., A. Niazi, and M. Kubista. 2005. Thermodynamics study of the dimerization equilibria of rhodamine B and 6G in different ionic strengths by photometric titration and chemometrics method. *Spectrochim. Acta A Mol. Biomol. Spectrosc.* 62:649–656.
50. Ilich, P., P. K. Mishra, …, T. P. Burghardt. 1996. Direct observation of rhodamine dimer structures in water. *Spectrochim. Acta A Mol. Biomol. Spectrosc.* 52:1323–1330.
51. Trick, J. L., E. J. Wallace, …, M. S. Sansom. 2014. Designing a hydrophobic barrier within biomimetic nanopores. *ACS Nano.* 8:11268–11279.
52. Trick, J. L., P. Aryal, …, M. S. Sansom. 2015. Molecular simulation studies of hydrophobic gating in nanopores and ion channels. *Biochem. Soc. Trans.* 43:146–150.
53. Duvvuri, M., Y. Gong, …, J. P. Krise. 2004. Weak base permeability characteristics influence the intracellular sequestration site in the multidrug-resistant human leukemic cell line HL-60. *J. Biol. Chem.* 279:32367–32372.
54. Gu, L. Q., S. Cheley, and H. Bayley. 2001. Prolonged residence time of a noncovalent molecular adapter, β-cyclodextrin, within the lumen of mutant α-hemolysin pores. *J. Gen. Physiol.* 118:481–494.
55. Kang, X. F., L. Q. Gu, …, H. Bayley. 2005. Single protein pores containing molecular adapters at high temperatures. *Angew. Chem. Int. Ed. Engl.* 44:1495–1499.
56. Valdes-Aguilera, O., and D. C. Neckers. 1989. Aggregation phenomena in xanthene dyes. *Acc. Chem. Res.* 22:171–177.
57. Gu, L. Q., and H. Bayley. 2000. Interaction of the noncovalent molecular adapter, β-cyclodextrin, with the staphylococcal α-hemolysin pore. *Biophys. J.* 79:1967–1975.
58. Khailova, L. S., D. N. Silachev, …, V. P. Skulachev. 2014. A short-chain alkyl derivative of Rhodamine 19 acts as a mild uncoupler of mitochondria and a neuroprotector. *Biochim. Biophys. Acta.* 1837:1739–1747.
59. Beckstein, O., and M. S. Sansom. 2003. Liquid-vapor oscillations of water in hydrophobic nanopores. *Proc. Natl. Acad. Sci. USA.* 100:7063–7068.
60. Karginov, V. A., E. M. Nestorovich, …, S. M. Hecht. 2007. Inhibition of *S. aureus* α-hemolysin and *B. anthracis* lethal toxin by β-cyclodextrin derivatives. *Bioorg. Med. Chem.* 15:5424–5431.
61. Ragle, B. E., V. A. Karginov, and J. Bubeck Wardenburg. 2010. Prevention and treatment of *Staphylococcus aureus* pneumonia with a β-cyclodextrin derivative. *Antimicrob. Agents Chemother.* 54:298–304.